Influence of the gravitational radius on asymptotic behavior of the relativistic Sitnikov problem

Juan D. Bernal,[1,*] Jesús M. Seoane,[1] Juan C. Vallejo,[1,2] Liang Huang,[3] and Miguel A. F. Sanjuán[1,4]

[1]*Nonlinear Dynamics, Chaos and Complex Systems Group, Departamento de Física, Universidad Rey Juan Carlos, Tulipán s/n, 28933 Móstoles, Madrid, Spain*

[2]*Joint Center for Ultraviolet Astronomy, AEGORA Research Group, Universidad Complutense de Madrid, Avda Puerta de Hierro s/n, 28040 Madrid, Spain*

[3]*Institute of Computational Physics and Complex Systems, School of Physical Science and Technology, Lanzhou University, Lanzhou 730000, China*

[4]*Department of Applied Informatics, Kaunas University of Technology, Studentu 50-415, Kaunas LT-51368, Lithuania*

(Received 31 May 2020; accepted 22 September 2020; published 7 October 2020)

The Sitnikov problem is a classical problem broadly studied in physics which can represent an illustrative example of chaotic scattering. The relativistic version of this problem can be attacked by using the post-Newtonian formalism. Previous work focused on the role of the gravitational radius λ on the phase space portrait. Here we add two relevant issues on the influence of the gravitational radius in the context of chaotic scattering phenomena. First, we uncover a metamorphosis of the KAM islands for which the escape regions change insofar as λ increases. Second, there are two inflection points in the unpredictability of the final state of the system when $\lambda \simeq 0.02$ and $\lambda \simeq 0.028$. We analyze these inflection points in a quantitative manner by using the basin entropy. This work can be useful for a better understanding of the Sitnikov problem in the context of relativistic chaotic scattering. In addition, the described techniques can be applied to similar real systems, such as binary stellar systems, among others.

DOI: 10.1103/PhysRevE.102.042204

I. INTRODUCTION

The three-body problem is a broadly studied subject in physics and classical mechanics [1]. Generally speaking, it consists in describing the dynamics of three point masses under mutual forces by the resolution of the correspondent equations of motion, taking into consideration the initial positions and velocities of the objects. It is well known that the three-body problem does not have a general analytic solution. Therefore, the use of numerical techniques is almost mandatory when we want to solve it. Although initially the three-body problem arose in the context of celestial mechanics, we may consider a three-body problem as any problem that models the motion of three particles due to their interaction forces, either gravitational or electromagnetic forces [2,3]. For example, the helium atom model, in which a helium nucleus and two electrons interact according to the inverse-square Coulomb interaction, is an analogue of the gravitational three-body problem in classical mechanics [4]. In fact, there are many simplifications and restricted cases of the three-body problem that allow us to get useful insights about real phenomena in nature without the need for solving more realistic and complex models. One of those paradigmatic models is the Sitnikov problem, which, despite its simplicity, has contributed to the understanding of the dynamics of motion of small bodies around eccentric primaries [5]. It consists of two primary bodies with the same mass which move in circular or elliptical orbits around their center of mass. Moreover, a third body, which is substantially smaller than the primary bodies, with negligible mass, moves under the gravitational interaction of the primary bodies along the z axis. For the sake of clarity, in this paper we call this particle a massless body, third body, or, simply, test particle.

The Sitnikov problem is a very illustrative first approach for testing mathematical techniques that can be applied later on to more realistic problems [6]. It is important to highlight that the Sitnikov problem is an unrealistic model. It is really useful for getting physical insights from interesting phenomena that may be described in nature, but the results cannot be directly extrapolated to real physical examples. From this point of view, the main flaws of the Sitnikov problem is that all the calculations depend on the unrealistic assumption that the planetoid moves only along the z axis. This is unrealistic since the z-axis orbit may be unstable with respect to transverse deviations, and even a very, very small initial transverse deviation in position or velocity builds up to a large lateral deviation within the time of the several hundred back and forth oscillations along the z axis. Taking this into consideration, we consider that some characteristics of the physical insights we have obtained in our work can be observed in nature. We can cite, for instance, scattering processes resulting when small bodies arrive nearly perpendicular to the orbital plane of a binary stellar system [7], or when one analyzes the flyby of an interstellar probe arriving perpendicular to the orbital plane of a planetary system [8]. It can also be seen as a first step in modeling the full motion of dust particles (with size larger than 1 μm) falling around an eccentric binary star, a star

*juandiego.bernal@urjc.es

orbiting a double-nucleus galaxy [9], or a Keplerian dumbbell satellite [10]. It is worthwhile noting that we will use the term Sitnikov problem or Sitnikov system in this paper to refer to the three-body problem aforesaid.

The Sitnikov system may be considered as a paradigmatic example of chaotic scattering since the massless body interacts with the region affected by the gravitational forces of the two primaries, and, while moving in the z axis due to the influence of the primaries, it may escape to infinity or may remain trapped in the scattering region forever. While it keeps in the scattering region, the particle may exhibit periodic and aperiodic oscillations as well as chaotic motions [11].

In general terms, chaotic scattering is defined as the interaction between an incident particle and a potential region or massive object that scatters it [12,13]. The equations of motion of the test particle modeling this interaction are nonlinear, and the resultant dynamics can be chaotic. Therefore, slightly different initial conditions may result in completely different trajectories. The region where the particle is affected by that potential field or massive object is called the scattering region. Outside the scattering region, the influence over the particle may be considered negligible and its motion is uniform and, essentially, free. On many occasions, the scattering region possesses different exits from which the particles may enter or escape after bouncing back and forth there for a while. In this case, we say that the system is open. From this point of view, chaotic scattering is regarded as a physical manifestation of transient chaos [14,15].

The scattering motion of the massless particle is originated by the gravitational forces from the primaries. The Newtonian equations can be considered a first approach as long as the velocities v of the bodies are small compared to the speed of light and $(\frac{v}{c})^2 = \beta^2 \ll 1$ [16]. The post-Newtonian formalism [17] finds an approximate solution to the field equations expressing the nonlinear Einstein's equations of gravity as a power series expansion, adding deviations from classical Newtonian dynamics with $(1/c)^2$ as an expansion parameter. The post-Newtonian approximation assumes weak gravity, slow motion of the matter, and internal energies in order to make a simultaneous expansion in small parameters characterizing these quantities. Only in the case of strong fields is it usually preferable to solve the complete equations numerically [18,19].

Previous works regarding relativistic chaotic scattering have studied the discrepancies between the predictions coming from the Newtonian laws of motion and special relativity, even for low velocities [20–23], because of the strong sensitivity to initial conditions of chaotic systems. In fact, discrepancies from the Newtonian and the relativistic schemes for low velocities are also present in relevant global properties of the chaotic scattering systems, such as the average escape time of the particles and the particle decay law [24]. Additionally, qualitative and quantitative differences in the topological character of the chaotic systems escape basins have been described as dependent on the effect of the Lorentz transformations [25].

Regarding the relativistic Sitnikov problem, the influence of the gravitational radius on the structure of the phase space portraits in the first post-Newtonian approximation was studied in Ref. [26]. However, the relativistic effects on many general properties of the chaotic system that give us crucial information about its asymptotic behavior predictability have received less attention. In chaotic systems we are not usually interested in the prediction of individual trajectories. Conversely, we may just want to know the final asymptotic state of the system.

In this context, we will refer here to the predictability of the system as the capacity to forecast this final state of a system. We will focus our work on characterizing the predictability of the massless particle in the relativistic Sitnikov problem, in the weak field approximation, when the post-Newtonian approximation is valid. The goal of this paper is to show that the asymptotic predictability of chaotic systems like this, characterized by its underlying escape basin topology, does depend on relativistic gravitational effects, even for weak fields. We also aim to show that this dependency is neither linear nor monotonous, but it is related to many subtle phenomena that take place in phase space.

This paper is organized as follows. In Sec. II we describe the Sitnikov problem in the first post-Newtonian approximation. A qualitative description of the gravitational effects of the primaries over the test particles' escape basin topology is shown in Sec. III. In Sec. IV we analyze two global properties of the Sitnikov system that characterize the prediction of the final state of the system: the decay law of the particles and the uncertainty dimension of a typical scattering function. We also describe here the changes in the KAM islands. In Sec. V we quantify the uncertainty of the system based on the study of the exit basin topology. We explain the results in the light of the analysis of the basin entropy. Last, in Sec. VI we discuss the influence of the gravitational radius over the predictability of the asymptotic behavior of the Sitnikov system as well as some physical applications.

II. DESCRIPTION OF THE RELATIVISTIC SITNIKOV PROBLEM

As mentioned in the Introduction, the Sitnikov problem is a special case of the three-dimensional restricted three-body problem, when the massless body moves along the z axis due to the gravitational effects of the primaries, although it has no influence on the inner dynamics of the primaries. From this point of view, the model description can be separated into two terms: the one describing the post-Newtonian approximation for the motion of the primaries, and the term modeling the dynamics of the massless particle due to the relativistic gravitational forces originated by the primaries. The post-Newtonian approximation for the primaries is based on the hypothesis that their gravitational interaction is weak and the orbital motions are slow. From this perspective, the equation of the relative motion of the primaries can be obtained from the Lagrangian given in Ref. [27],

$$\frac{\mathbf{d^2r}}{\mathbf{dt^2}} = \frac{\mathbf{dv}}{\mathbf{dt}} = -\frac{\mathbf{r}}{r^3} + \lambda\Bigg[-(1+3\nu)\frac{\mathbf{r}}{r^3}v^2 + \frac{3}{2}\nu\frac{\mathbf{r}}{r^5}(\mathbf{rv})^2 + (4+2\nu)\frac{\mathbf{r}}{r^4} + (4-2\nu)\frac{\mathbf{r}}{r^3}(\mathbf{rv})\Bigg], \tag{1}$$

where $\mathbf{r}$ and $\mathbf{v}$ are, respectively, the vectors characterizing the relative position and the relative velocity of the primaries. The

parameter $\nu = m_1 m_2/(m_1 + m_2)^2$ measures the difference between the masses of both primaries, m_1 and m_2. In the Sitnikov system described here $m_1 = m_2 = m$, therefore, $\nu = 1/4$. The dimensionless gravitational radius λ is defined as

$$\lambda = \frac{2km}{ac^2}, \tag{2}$$

where a is the classical semimajor axis of the orbit, k represents the gravitational constant, and c is the speed of light. Therefore, we may say that the parameter λ is the one that gathers the gravitational effects of the primaries over the spacetime, including any object allocated in the spacetime as the massless particle.

For convenience, the classical semimajor axis a will be the selected unit length,

$$a = \frac{-km^2}{2E_c}, \tag{3}$$

where E_c is the classical energy in the center of the mass frame. The energy unit is taken as km^2/a. Therefore, in these units, the classical energy is $E_c = -0.5$. Likewise, according to Kepler's third law, the time unit is $T = a^{3/2}[2km]^{-1/2}$.

The Lagrangian used to derive Eq. (1) is invariant under translations and rotations, which implies the existence of four integrals. The total energy of the primaries in the center-of-mass frame is given by

$$E = \frac{1}{2}v^2 - \frac{1}{r} + \frac{\lambda}{2}\left\{\frac{3}{4}(1-3\nu)v^4 + \frac{1}{r}\left[(3+\nu)v^2 + \nu\frac{(\mathbf{r}v)^2}{r^2} + \frac{1}{r}\right]\right\}, \tag{4}$$

and the angular momentum is

$$\mathbf{J} = \mathbf{r}\times\mathbf{v}\left\{1 + \lambda\left[\frac{1}{2}(1-3\nu)v^2 + (3+\nu)\frac{1}{r}\right]\right\}. \tag{5}$$

The conservation of the angular momentum $\mathbf{J}$ implies that the motion of the primaries takes place always on a two-dimensional surface.

On the other hand, the classical eccentricity is defined as

$$e_c = \left[1 - J_c^2\right]^{1/2}, \tag{6}$$

where J_c is the classical angular momentum, that is, $\mathbf{J_c} = \sum \mathbf{r_i}\times m_i\mathbf{v_i}$.

Finally, the equation of motion of the massless body is obtained from the Lagrangian of the post-Newtonian three-body system as [26]

$$\frac{d^2z}{dt^2} = -\frac{z}{\rho^3} + \lambda\left[\frac{5}{4}\frac{z}{r\rho^3} + \frac{16}{2}\frac{z}{\rho^4} - \frac{v^2 z}{\rho^3} + 6\frac{v_z^2 z}{\rho^3} + \frac{3}{2}\frac{(\mathbf{v}r)v_z}{\rho^3} + \frac{3}{16}\frac{(\mathbf{v}r)^2 z}{\rho^5}\right], \tag{7}$$

where z and v_z are the position and the velocity module of the massless body, respectively. The parameter $\rho = \sqrt{z^2 + (r^2/4)}$ depends on the position of the massless body and the relative position of the primaries. In Fig. 1 we see a schematic drawing of the Sitnikov problem. In this paper, we have chosen the value $\mathbf{r}_{\text{peric}} = (1 - e_c, 0)$ with $e_c = 0.2$, as the initial condition for the position the primaries, where the variable $\mathbf{r}_{\text{peric}}$ denotes the pericenter of the elliptic movement. Likewise, the initial velocity of the relative position of the primaries is $v = [0, \sqrt{(1+e_c)/(1-e_c)}]$. For the massless particle, the initial conditions are given by the pair (z, v_z).

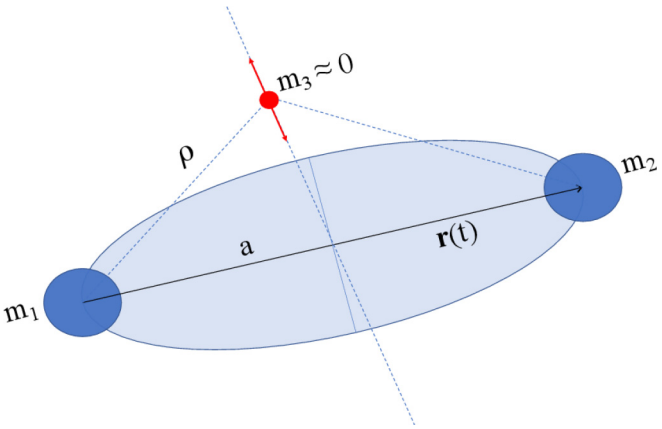

FIG. 1. Schematic configuration of the Sitnikov problem. Two primary bodies with the same mass ($m_1 = m_2 = m$) move in circular or elliptical orbits around their center of mass. A third body, substantially smaller than the primary bodies ($m_3 \approx 0$), moves under the gravitational interaction of the primary bodies in a line that is perpendicular to the orbital plane of the primary bodies. Therefore, the third body moves in only one dimension along the z axis. The parameter a is the semimajor axis, $\mathbf{r}$ is the relative position of the primaries, and ρ is the relative position of the massless body with regard to the primaries, $\rho = \sqrt{z^2 + (r^2/4)}$.

In order to solve Eq. (7) we need to know the time-dependent value of the relative position $\mathbf{r}$ and velocity $\mathbf{v}$ of the primaries. Therefore, the solution of Eq. (1) provides the time-dependent driving for the relativistic Sitnikov problem.

Figure 2 illustrates the effects of the gravitational radius λ on the chaotic dynamic of the massless particle according to Eq. (7). We can see the evolution of the relative vector position $\mathbf{r}$ in the plane (x, y) and the trajectory of the massless particle in the phase space (z, v_z), for different values of λ. All trajectories in this figure have the same initial condition, $(z, v_z) = (1, 0)$. The leftmost panels represent the position of the relative vector of the primaries, and the rightmost panels the phase portrait of the massless particle. Figures 2(a) and 2(b) are plotted using $\lambda = 0.01$. The massless particle exhibits a periodic motion, and it never leaves the scattering region. Likewise, in Figs. 2(c) and 2(d), we show the relative motion of the primaries and the test particle for $\lambda = 0.035$. In this case, the massless particle leaves the scattering region quickly.

Following Ref. [26], the numerical results for the post-Newtonian approximation are just valid in the range $\lambda \in (0, 0.035]$. For higher values of the gravitational radius, the post-Newtonian approximation of the two-body problem differs from the analytical results in more than 10%. For this reason, the maximum value considered for gravitational radius in this research is $\lambda = 0.035$.

III. GRAVITATIONAL EFFECTS OF THE PRIMARIES DYNAMICS ON THE TEST PARTICLE ESCAPE BASINS

As we have seen in the previous section, two planetoids, with similar initial conditions z, v_z, may have different

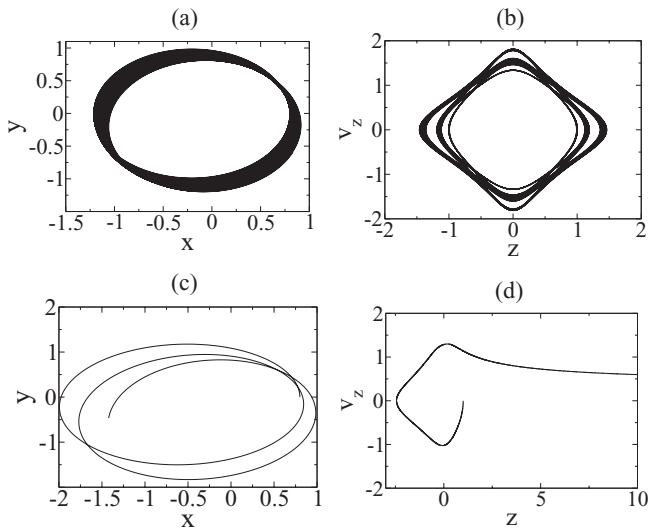

FIG. 2. Relative trajectories of the primaries (left panels) and the test particle (right panels) for different values of the gravitational radius λ. The initial condition for the massless particle is $(z, v_z) = (1, 0)$. Panels (a) and (b) use $\lambda = 0.01$: the test particle has a periodic motion, and it remains in the scattering region forever. Panels (c) and (d) use $\lambda = 0.35$: the massless test particle leaves the scattering region quickly.

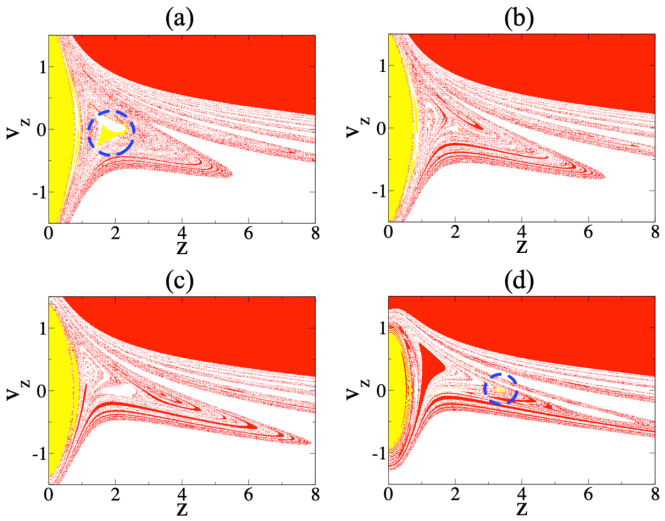

FIG. 3. Evolution of the exit basins of the Sitnikov system for different values of the gravitational radius λ. The sets of red and white dots denote initial conditions resulting in trajectories that escape through Exit 1 (to $z \to +\infty$) and Exit 2 (to $z \to -\infty$). The yellow regions are the initial conditions which do not escape. As we are drawing the range $z \in [0, 8]$, the pictures show asymmetry and the particle bias for escaping to $+\infty$ when they are shot from $v_z \in (0, +1.5)$ and to escape to $-\infty$ when shot from $v_z \in (0, -1.5)$. (a) A very low gravitational radius, $\lambda = 1 \times 10^{-5}$: the exit basins are quite mixed throughout the central region of the phase space, and there is a KAM island that can be easily recognized around $z \simeq 2.0$. We have highlighted this area with a blue circle. (b) $\lambda = 0.01$: the KAM island at $z \simeq 2$ has disappeared, and the exit basins are still fairly mixed in the central region. There can be seen bigger regions of particles escaping by Exit 1 and Exit 2 in that central region. (c) $\lambda = 0.02$: the exit basin regions are larger in the central region. The exit basin boundaries are still fractal. There are no KAM islands apart from the big yellow area, which corresponds to the stable region surrounding $z = 0$. (d) $\lambda = 0.035$: the exit basins in the central region are bigger, and the boundaries are fractal. There is a new stable region of trapped particles at $z \simeq 3.7$ (surrounded by a blue circle). The large KAM island surrounding $(z, v_z) = (0, 0)$ has decreased ostensibly.

transient trajectories due to the gravitational influence of the primaries. Here we deal with the gravitational effect of the dynamics of the primaries over the asymptotic behavior of the test particle, as is reflected in the structure of the corresponding escape basins.

In Hamiltonian systems, we define an exit basin or escape basin as the set of initial conditions whose trajectories converge to an specific exit [28]. In the specific case of the Sitnikov problem, the massless particle moving along z axis may escape upwards (to $+\infty$), hereafter called Exit 1, or downwards (to $-\infty$), called Exit 2. In addition, it may also remain in the scattering region, bouncing back and forth along the z axis forever. Therefore, the massless particle has three possible asymptotic behaviors: remaining in the scattering region forever, escaping by Exit 1, or escaping by Exit 2.

Generally speaking, we say that an initial condition g is a boundary point of a basin B if every open neighborhood of g has a nonempty intersection with basin B and at least one other basin. The basin boundary is the set of all boundary points of that basin. The basin boundary could be a smooth curve, but in chaotic systems the boundaries are usually fractal. In that case, those fractal structures impose an extremely sensitive dependence on the initial conditions, which obstructs the prediction of the system final state. For that reason, the understanding of the exit basin topology is crucial to foresee the final fate of the system.

In order to determine the escape basins of the relativistic Sitnikov system, we integrate 10^6 particles during a maximum time $T_{\max} = 300$ time units, regularly shot over the range $z \in [0, 8]$, with initial velocities in the interval $v_z \in [-1.5, 1.5]$. Then we follow each trajectory and we register by which exit the particles have escaped from the scattering region. If a particle leaves this region by Exit 1, then we color the initial condition in red. Likewise, we color the initial condition in white if the particle escapes by Exit 2. Finally, when a particle remains in the scattering region up to the maximum computation time, we color its initial condition in yellow. We may consider that the condensed yellow regions are KAM islands, and, in those regions the motion of the test particles remain quasiperiodic. The rest of the yellow points that are spread throughout the phase space are boundary points.

We have run different simulations to plot the exit basins of the Sitnikov system for a wide range of the gravitational radius λ values. The evolution of these exit basins is seen in Fig. 3. Figure 3(a) represents the case of influence of a very low gravitational radius, $\lambda = 1 \times 10^{-5}$. It corresponds almost to the Newtonian case. There is a large KAM island corresponding to the stable region surrounding $z = 0$. There is also another KAM island that can be easily recognized as the yellow area in $z \simeq 2.0$. For the sake of clarity, we have highlighted this area with a blue circle. The exit basins are

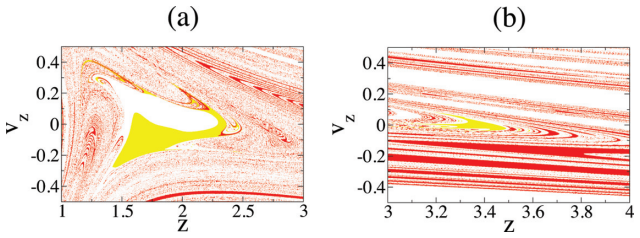

FIG. 4. Magnification of the KAM islands from Figs. 3(a) and 3(d). The sets of red and white dots denote initial conditions resulting in trajectories that escape through Exit 1 (to $z \to +\infty$) and Exit 2 (to $z \to -\infty$). The yellow regions are the initial conditions which do not escape. (a) Zoom-in of Fig. 3(a) for the region $v_z \in [-0.5, 0, 5]$ and $z \in [1, 3]$. (b) Zoom-in of Fig. 3(b) for the region $v_z \in [-0.5, 0, 5]$ and $z \in [3, 4]$.

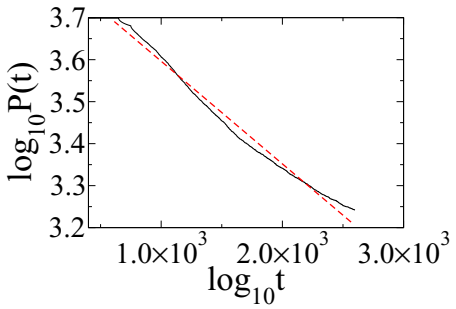

FIG. 5. Algebraic decay law of the system for $\lambda = 0.02$. 10 000 particles are shot towards the scattering region from $z \in (0.5, 8.0)$ and initial velocity $v_z = 0$. We get the fraction of particles inside the scattering region between t and $t + dt$, and we represent $\log_{10}P(t)$ vs $\log_{10}t$. The slope of the red dotted straight line is the exponent of the decay law, the parameter κ [see Eq. (8)].

quite mixed throughout the central region of the phase space. In Fig. 3(b) we can see the relativistic effects of the gravitational radius when $\lambda = 0.01$. The KAM island at $z \simeq 2$ is not present anymore, and the exit basins are still fairly mixed in the central region. In Fig. 3(c) we represent the exit basins of the system for $\lambda = 0.02$. One can see bigger regions of particles escaping by Exit 1 and by Exit 2 in the central region. The exit basins are still quite mixed, and the boundaries are fractal. Last, in Fig. 3(d) we show the Sitnikov exit basins for $\lambda = 0.035$. The exit basins are still fairly mixed on the phase space although the escape regions are larger. The fractality of the boundaries has decreased. Apart from that, the main novelty from the previous cases is the appearance of a new KAM island at $z \simeq 3.7$ (surrounded by a blue circle). This is a transition of the KAM island in the phase space due to the variation of the parameter λ. Our numerical findings point out this change in the topology of the escape basins to occur from $\lambda \simeq 0.0285$ until $\lambda \simeq 0.0350$. It is also important to note that the large KAM island surrounding $(z, v_z) = (0, 0)$ has decreased ostensibly. In order to see in more detail the qualitative effects of the variation of λ in the creation and destruction process aforesaid described, we show in Fig. 4 the zoom-ins from Fig. 3 in the areas surrounding the KAM islands.

As we can see, the relativistic gravitational effect of the primaries over the test particle is very relevant since it modifies the exit basin topology of the system. These changes will be discussed in detail in the following sections.

IV. KAM ISLAND METAMORPHOSIS AND CROSSOVER PHENOMENON

We have seen in a qualitative manner how the asymptotic behavior of the test particles, represented by the exit basins, is affected by the variation of the gravitational radius of the primaries λ. In this section we will use the uncertainty dimension as quantitative tool to determine that transformation process and to extract more physical insights about the asymptotic predictability of the Sitnikov system.

First, we need to introduce the concept of time delay statistics. Suppose that we pick many different initial conditions at random in some interval of the domain. Then we examine the resulting trajectory for each value and determine the time t that its trajectory spends in the scattering region. The fraction of trajectories with time delay between t and $t + dt$ is $P(t)dt$. For open nonhyperbolic dynamics with bounding KAM surfaces in the scattering region, one finds that for large t the time delay statistics, $P(t)$, decays algebraically as

$$P(t) \sim t^{-\kappa}, \tag{8}$$

where κ is the exponent of the algebraic decay law, and it is directly related to the speed of escape of the particles. As we saw in Sec. III, there is a large KAM island surrounding $z \approx 0$ for all λ. Apart from that, there is a KAM island at $z \simeq 2.0$, in the interval $\lambda \in (0, 0.01)$, and, after the metamorphosis process $\lambda \simeq 0.0285$, there is a new KAM island at $z \simeq 3.7$. Therefore, we may state that the Sitnikov system exhibits a nonhyperbolic regime for the whole range of energies and initial conditions we have considered, and the decay law is algebraic.

We have considered here 10^4 particles shot towards the scattering region with $z \in (0.0, 8.0)$ and initial velocity $v_z = 0$. Then we get the fraction of particles $P(t)dt$ inside the scattering region between t and $t + dt$. Now, we represent $\log_{10}P(t)$ versus $\log_{10}t$. The value of the parameter κ is the slope of the resulting straight line, according to Eq. (8). To illustrate this, we show in Fig. 5 the algebraic decay law represented by $\log_{10}P(t)$ versus $\log_{10}t$ for $\lambda = 0.02$.

We have computed the parameter κ for different values of the gravitational radius λ. In Fig. 6 we show the evolution of κ with λ. A blue (black) line is used to help the eye to get a better insight into the trend of the points.

As we can see, the value of the parameter κ decreases from $\lambda = 0.0$ to $\lambda \simeq 0.005$. Here the particles, in average, stay in the scattering region longer. Afterwards, the value of the exponent κ grows in the interval $\lambda \in (0.005, 0.02)$. Indeed, κ reaches a maximum around $\lambda \simeq 0.02$. That means the particles stay in the scattering region shorter and escape sooner than before. Finally, as the λ values keep growing from $\lambda \approx 0.02$ to $\lambda \approx 0.035$, κ decreases. We consider that the variation process of κ with λ is mainly governed by the evolution of the KAM island topology with λ. The KAM islands exhibit the stickiness property, in the sense that its presence in the phase space leads to longer transients of the particles inside the scattering region [29]. As we will see later, changes in the

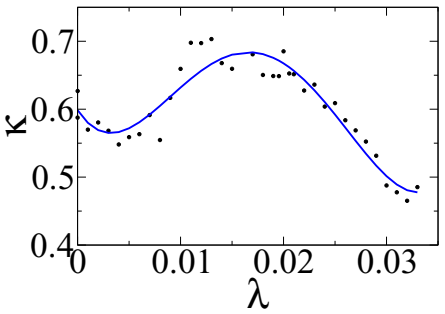

FIG. 6. Influence of the gravitational radius λ over the exponent of the decay law κ. 10 000 particles are shot towards the scattering region from $z \in (0.5, 8.0)$ and initial velocity $v_z = 0$. We calculate the parameter κ, that is, the slope of the straight line $\log_{10}P(t)$ vs $\log_{10}t$ (as it was illustrated in Fig. 5) for different values of the gravitational radius λ. A blue line is used to help the eye to get a better insight into the trend of the points. The value of the parameter κ decreases in the interval $\lambda \in (0.0, 0.005]$. It grows from $\lambda \simeq 0.005$, and it reaches a maximum value around $\lambda \simeq 0.02$, then it decreases in the range $\lambda \in (0.02, 0.035]$. The reason behind this behavior is the process of destruction of the KAM island at $z \simeq 2.0$ and the creation of a new one due to the variation of the gravitational radius λ.

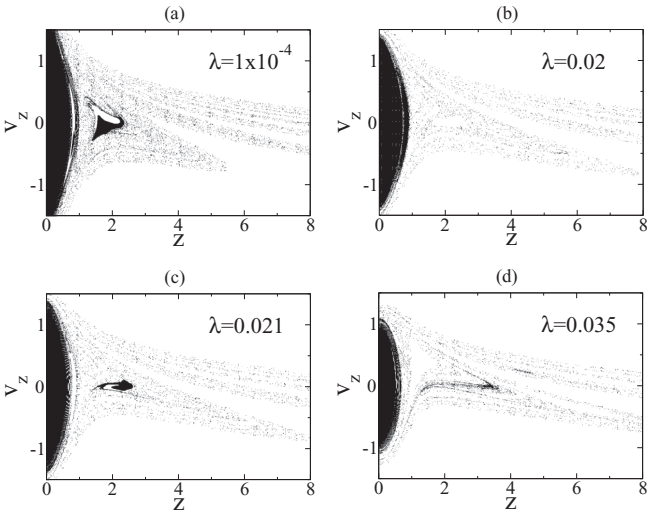

FIG. 7. Evolution of the particles that are trapped in the scattering region after $T_{\max}$ for different values of the gravitational radius λ. Black dots are the initial conditions which do not escape. To generate the plots, we launched 1 000 000 particles from the set of initial conditions (z, v_z) in $[0, 8] \times [-1.5, 1.5]$. (a) $\lambda = 1 \times 10^{-5}$: there is a big black region surrounding $z = 0$ and a large KAM island around $z \simeq 2.0$. (b) $\lambda = 0.02$: no KAM islands are in the phase space, and there are fewer trapped particles in the phase space although they are still all over the central region. (c) $\lambda = 0.0207$: a new KAM island appears at $z \simeq 2.5$. Just a small variation in λ provokes an important variation of the phase space topology. (d) $\lambda = 0.035$: there is a new stable region of trapped particles at $z \simeq 3.7$. This KAM island grows from $\lambda \simeq 0.0285$ to $\lambda = 0.0355$. We can see the manifestation of the metamorphosis phenomenon taking place in phase space due to the increasing of the parameter λ.

gravitational radius values lead to the creation, modification, and destruction of the KAM islands in the phase space.

In order to better illustrate the relation between the evolution of κ with λ, we show in Fig. 7 the escape basin evolution of the trapped particles with the gravitational radius λ. We use the same conditions used to obtain Fig. 3, but now we represent only the particles that do not escape from the scattering region (represented by the black dots). In Fig. 7(a) we represent the trapped particles of the Sitnikov system for $\lambda = 1 \times 10^{-5}$. There is a large black area which corresponds to the stable region surrounding $z = 0$, and there also is a large KAM island in $z \simeq 2.0$. In Fig. 7(b) we can see that the aforesaid KAM island at $z \simeq 2$ no longer exists for $\lambda = 0.02$. Indeed, it does not exist in $\lambda \in (0.005, 0.02]$. Many trapped particles are spread along the central region of the phase space. These are the initial conditions laying in the basin boundaries. In Fig. 7(c) we can see the effects of the gravitational radius at $\lambda = 0.02$. There are no KAM islands apart from the big one centered at $(z, v_z) = (0, 0)$, and there are fewer trapped particles spread over the phase space. It is a qualitative expression of the decay in the boundary fractality. However, just at a slightly higher value of the gravitational radius, $\lambda = 0.0207$, a new KAM island appears at $z \simeq 2.5$. Therefore, it demonstrates that a small variation in the gravitational radius provokes a relevant change in the topology of the phase space. It is also worth noting that, from $\lambda \simeq 0.02$ to $\lambda \simeq 0.0285$, there are two processes that take place in parallel: the destruction of the recently created KAM island at $z \simeq 2.5$ and the creation of another KAM island at $z \simeq 3.7$. This last KAM island grows from $\lambda \simeq 0.0285$ to $\lambda = 0.0355$. In Fig. 7(d), corresponding to the case of $\lambda = 0.035$, the KAM island can be easily identified in the phase space at $z \simeq 3.7$.

These figures show that the variation of the gravitational radius yields to different transformations in the phase space, and it hinders the predictability of the final state of the system. In order to quantify the evolution of the predictability of this asymptotic behavior, we use one fundamental feature of any chaotic system, the scattering function. The scattering function relates an input variable of the incident particle with an output variable that characterizes the trajectory of the particle, once the scattering phenomenon takes place. These scattering functions can be obtained empirically and are useful to infer relevant information about the system.

In Fig. 8 we can see a typical scattering function for the Sitnikov system. It shows the average escape time of a test particle when it is shot from different values of initial position z. The initial velocity in all cases is $v_z = 0.5$, and the gravitational radius is fixed to $\lambda = 0.03$. We use two panels to represent the scattering function. The lower left panel shows the scattering function for a range of initial positions $z \in [1.5, 3.0]$. The upper right panel is a magnification of the scattering function, just varying the initial position in a narrower range, $z \in [1.9, 2.0]$. In Fig. 8 we can see that the scattering function contains some regions where the escape time of the particle varies smoothly with z, while there are some other fractal regions with singularities. This pattern is present in both scales, being a qualitative insight of the self-similarity of the fractal regions.

In the fractal regions of the scattering functions, any small variation in the neighborhood of the input variable z implies a huge variation in the output variable, which in our case is the escape time T_e. Moreover, this variation of the output variable

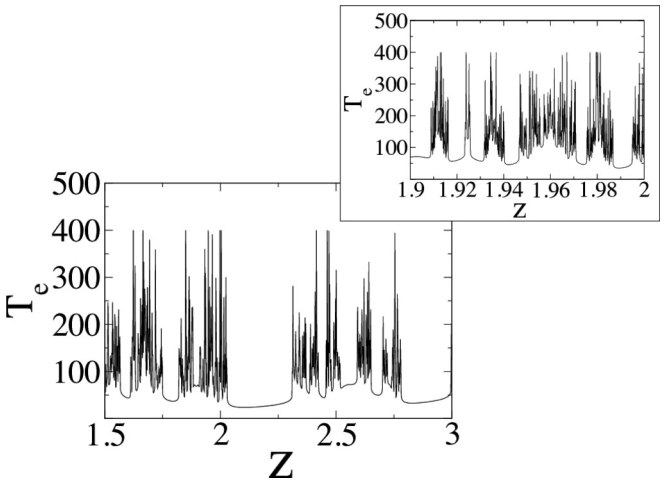

FIG. 8. Typical scattering function of the escape time T_e vs the initial position z of 10^3 particles shot into the scattering region with initial velocity $v = 0.5$. The gravitational radius is $\lambda = 0.03$. The lower left panel shows the scattering function for the initial position $z \in [1.5, 3.0]$. On the other hand, the upper right panel is a zoom-in of the scattering function, taking a narrower initial position range, $z \in [1.9, 2]$. The scattering function contains some regular regions where the escape time varies with z in a smoothly manner. However, there are others where a slightly different initial condition implies an abrupt change in the particle escape time.

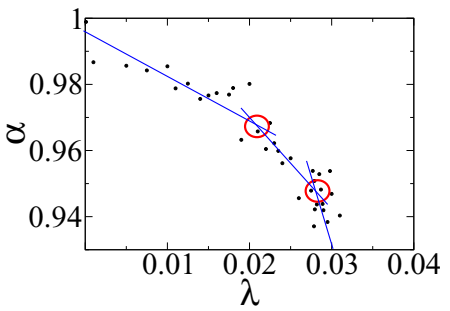

FIG. 9. Evolution of the uncertainty dimension α in a scattering function defined on the initial line segment at $z_0 = [1.5, 2.5)$ with the variation of the gravitational radius λ. For many values of $\lambda \in (0, 0.035]$ we randomly launch 1000 test particles from that line segment. The particles are shot towards the scattering region with initial velocity $v = 0.5$. The results point out three different regions in the figure, First, there is a linear decay in the range $\lambda \in (0, 0.020)$. Then, at $\lambda \simeq 0.02$, there is an inflection point. Later, there is an abrupt decay of the uncertainty dimension α, at $\lambda \simeq 0.0285$. At this point, there is a crossover behavior since, for values $\lambda > 0.0285$, there is a drop of α.

does not tend to zero when the variation of z goes to zero. This type of behavior of the scattering function means that a small uncertainty in the determination of the input variable could make impossible any prediction about the future value of the output variable. For this reason, the fractal dimension of the set of values of singular input variables provides a quantitative characterization of the magnitude of this uncertainty. That is why the fractal dimension α is also typically defined as the uncertainty dimension.

Here we investigate the evolution in a typical scattering function of the uncertainty dimension α as λ changes. We have used the uncertainty algorithm from Ref. [30], in order to compute α. We select a certain interval in the z axis, $z \in [1.5, 2.5)$, from which we shoot the test particles towards the scattering region with initial velocity $v = 0.5$. For a certain initial condition on the line segment, i.e., z_0, we choose a perturbed initial condition $z_0' = z_0 + \chi$, where χ is the amount of perturbation. For convenience, in our calculations we choose $\chi \in [1 \times 10^{-8}, 1 \times 10^{-1})$. Then we let both trajectories evolve according to Eq. (7). We track the time they spend in the scattering region and by which exit they escape. In the case that two trajectories escape from the scattering region at the same time or throughout the same exit, we consider that the trajectories are certain with regard to the perturbation χ. Otherwise, we say the trajectories are uncertain. After taking a large number of initial conditions for each value of χ, the fraction of uncertain initial conditions $f(\chi)$ scales algebraically with χ as $f(\chi) \sim \chi^{\alpha}$. Therefore, α is the so-called uncertainty dimension. Due to the algebraic scaling, if the boundary is fractal, then $\alpha < 1$. Any improvement of the initial condition accuracy by, for instance, a factor of 10 reduces $f(\chi)$ by a factor much less than 10. That is why we say there is a final state sensitivity, and the situation with respect to the potential improvement predicted by increasing initial condition accuracy is less favorable the smaller α is.

Figure 9 plots the evolution of the uncertainty dimension α with different values of the gravitational radius λ, with the blue lines showing the general decreasing trend in the whole range $\lambda \in [0, 0.035]$. We can distinguish three different regions. First, there is a linear decay in the range $\lambda \in (0, 0.020)$. Then, there is an inflection point at $\lambda \simeq 0.02$ where the slope of the line changes. Later, at $\lambda \simeq 0.0285$, there is an abrupt decay of the uncertainty dimension α. These three regions are directly related to the influence of the variation of the gravitational radius over the exit basin topology and the related creation and destruction of KAM islands. This is also highlighted in Figs. 6 and 7.

We can gain insight into the dependence of the uncertainty dimension α with the parameter λ, by following the approach described in Ref. [31]. We consider the iterative construction of the middle-third Cantor set so that at the nth iteration there are $N = 2^n$ intervals, each of length $\epsilon_n = 2^{-n}[2/(n+2)]$. The middle-third Cantor set possesses a Lebesgue measure zero and a fractal dimension equal to 1.

The total length of all the intervals is $\epsilon_n N \sim n^{-1}$, and it goes to zero as n goes to infinity. The required number of intervals of size ϵ_n that are needed for covering the set is $N(\epsilon) \sim \epsilon^{-1}(\ln \epsilon^{-1})^{-1}$. The fractal dimension is defined as $\alpha = \lim_{\epsilon \to 0}[\ln(N(\epsilon))/\ln(\epsilon^{-1})]$, which clearly yields 1. The exponent of the dependence $N(\epsilon) \sim 1/\epsilon^{\alpha}$ is the uncertainty dimension α.

Despite the fact that the weaker logarithmic term does not have any influence on the determination of the dimension, this term is the one that makes the Cantor set to be a Lebesgue measure zero since $\epsilon N \sim (\ln \epsilon^{-1})^{-1}$ tends to 0 as $\epsilon \to 0$.

In order to generalize this example, we may consider that in each stage we remove a fraction $\eta_n = a/(n+b)$, where a and b are constants, from the middle of each of the 2^n remaining

intervals. Then we find that

$$N(\epsilon) \sim (1/\epsilon)[\ln(1/\epsilon)]^{-a}. \tag{9}$$

According to Eq. (9), the slope at any point of the curve $\ln N(\epsilon)$ versus $\ln(1/\epsilon)$ is, by definition, $d \ln N(\epsilon)/d \ln(1/\epsilon)$, and it is always less than 1 for small ϵ, although it approaches 1 logarithmically as $\epsilon \to 0$. Therefore, the result about the fractal dimension is still $\alpha = 1$.

Now, we can do a parallelism between the fractal dimension of Cantor-like structures and the relativistic Sitnikov problem we are studying. First, we note that chaotic scattering occurs due to a nonattracting chaotic set (i.e., a chaotic saddle) in phase space where the scattering interactions take place [32]. Moreover, both the stable and the unstable manifolds of the chaotic saddle are fractals [33].

The scattering particles are launched from a line segment straddling the stable manifold of the chaotic saddle outside the scattering region [34]. The set of singularities is the set of intersections of the stable manifold and the line segment, and it can be effectively considered a Cantor-like set.

There is an interval of the input variables which leads to some trajectories that remain in the scattering region for at least a duration T_0. By time $2T_0$, there is a fraction η of these particles leaving the scattering region. In the case that these particles are all located in the middle of the original interval, there are then two equal-length subsets of the input variable that lead to trajectories that remain in the scattering region for, at least, $2T_0$.

Likewise, we may consider that a different fraction η of incident particles, whose initial conditions were located in the middle of the first two subintervals that remain at time $2T_0$, are now leaving the scattering region by $3T_0$. There are then four particle subintervals that remain in the scattering region for at least $3T_0$.

If we continue this iterative procedure, we can easily recognize a parallelism of the emerging fractal structure produced by the particles that never escape and a Cantor-like set of zero Lebesgue measure.

The fractal dimension α of the Cantor set then is given by

$$\alpha = \frac{\ln 2}{\ln[(1-\eta)/2]^{-1}}. \tag{10}$$

As we have previously seen, the time delay statistics of the particles, $P(t)$, decays in an algebraic fashion in the nonhyperbolic regime. This implies that the fraction η is not constant during the iterative process of construction of the Cantor set. At the nth stage (being n large enough), the fraction η_n is approximately given by

$$\eta_n \approx -T_0 P^{-1} dP/dt \approx \kappa/n. \tag{11}$$

This expression obviously yields a Cantor set with dimension $\alpha = 1$ when we substitute $\eta_n \approx \kappa/n$ in Eq. (10).

If we compare this result with the mathematical expression obtained for the middle-third Cantor set as shown in Eq. (9), then we realize that the exponent κ of the algebraic decay law corresponds to the exponent a of Eq. (9).

Taking this into consideration, we obtain the relation

$$\alpha = \frac{\ln 2}{\ln\left(\frac{2}{1-\kappa/n}\right)}, \tag{12}$$

which explains the behavior observed in Fig. 9. As $\lambda \to 0$, we have $\alpha \to 1$ for large n. Moreover, when $\lambda \to 0$, we obtain that $d\alpha/d\lambda \approx 0$, recovering the Newtonian system. When λ increases, α decreases, and for large values of n, the value of α is always between 0 and 1 because the exponent κ of the algebraic decay law is bound $\in (0.52, 0.72)$ for the range $\lambda \in (0, 0.035)$, as we noted in Fig. 6.

We have seen here how the asymptotic behavior of the Sitnikov system can become less predictable under the influence of the gravitational radius. This has been illustrated with the evolution of the decay law of the particles with λ, when the KAM islands are created and destroyed in the phase space.

These changes are related to having longer or shorter transients in the scattering region. Being the uncertainty dimension α a decreasing function with the gravitational radius λ, we can state that the system is more unpredictable when λ values are higher. Moreover, the relation of the uncertainty dimension with the gravitational radius is not monotonous, which makes the prediction more difficult. Conversely, it presents inflection points which reflect the changes taking place in phase space and the KAM islands.

V. QUANTIFICATION OF THE ASYMPTOTIC PREDICTABILITY EVOLUTION DUE TO THE GRAVITATIONAL RADIUS VARIATION

In this section we quantify the lack of predictability of the Sitnikov system due to the influence of primaries on the test particles. For that purpose, we will characterize the changes in the escape basin topology using the concept of basin entropy [35]. The basin entropy is based on the discretization of the continuous phase space of the system in a discrete grid. This discretization is valid because any experimental or numerical procedure to determine any point of the phase space has a finite resolution.

Considering the same exit basins of the Sitnikov system seen in Fig. 6, we can easily create a discrete grid if we assume a finite precision δ in the determination of the initial conditions. When we cover the phase space with boxes of size δ, every piece of the grid is surrounded by other pieces, and we may define a ball around each piece as the pieces share some side with it.

For computing the basin entropy, this ball can be taken as a random variable, with the potential results of the different exit basins. Considering that the pieces inside the ball are independent and applying the concept of Gibbs entropy, the basin entropy S_b is defined as

$$S_b = \sum_{k=1}^{k_{\max}} \frac{N_k^0}{N^0} \delta^{\alpha_k} \log(m_k), \tag{13}$$

where k is the label for the different exit basin boundaries, m_k is the number of exit basins contained in a certain ball, and α_k is the uncertainty dimension of the boundary k as defined in Sec. IV. The ratio N_k^0/N^0 is a term related with the portion of the discretized phase space occupied by the boundaries, that is, the number of pieces lying in the boundaries divided by the total number of pieces in the grid.

Therefore, there are three sources that increase the basin entropy: (1) N_k^0/N^0, that is, the larger portion of the phase

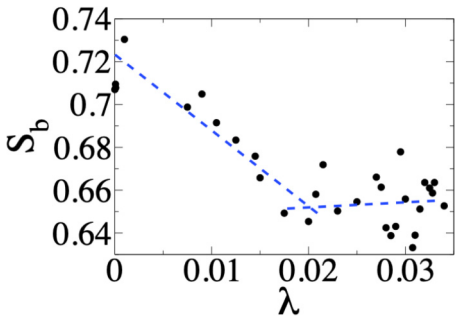

FIG. 10. The figure shows the evolution of the basin entropy S_b of the relativistic Sitnikov system with λ. There are two regions where S_b evolves differently. In the range $\lambda \in (0, 0.02]$ there is a linear decrease of the basin entropy S_b with λ, while in the range $\lambda \in (0.0, 0.035]$ there is an almost flat variation of S_b with λ.

space occupied by the boundaries, the higher S_b; (2) the uncertainty dimension term δ^{α_k}, related to the fractality of the boundaries; and (3) $\log(m_k)$, which is a term related to the number of different exit basins m_k.

In Fig. 10 we can see the evolution of the basin entropy S_b of the Sitnikov system with the gravitational radius λ. First, there is a linear decrease of the basin entropy S_b with λ within the range $\lambda \in (0, 0.02)$. In this region, there are fewer pieces in the grid of the discretized phase space occupied by the boundaries, as can be seen in panels (a–c) from Figs. 3 and 6. Therefore, the ratio N_k^0/N^0 decays within that range of λ. Moreover, in $\lambda \in (0, 0.02)$, the uncertainty dimension also decreases as λ is increased, as can be seen in Fig. 10. Then the second source of variation of S_b, the uncertainty dimension term δ^{α_k}, is reduced as λ grows. As long as $\lambda \gtrsim 0.02$, there is greater dispersion in the values of the basin entropy. However, we see a linear and almost flat variation of S_b with λ.

The observed dispersion is a clear signal of the creation and destruction of KAM islands in phase space [36]. We consider that this is the result of the added effects of both inflection points in the uncertainty dimension α at $\lambda \simeq 0.02$ and $\lambda \simeq 0.0285$, and the growth of the term N_k^0/N^0 since there are more pieces in the grid of the discretized phase space occupied by the boundaries in the range $\lambda \in (0.02, 0.035]$.

We consider that the evolution of the basin entropy S_b with α shown in Fig. 10 reinforces the conclusions reached in the previous sections: changes in the gravitational radius λ make the Sitnikov system more unpredictable, as reflected by the dispersed values of the basin entropy we have computed.

VI. CONCLUSIONS AND DISCUSSION

Relevant progress in understanding special relativity effects on chaotic scattering has been observed in the past few years. Most of the results have been focused on studying the trajectories of single particles when the relativistic approach is taken into consideration. More recently, some works have also demonstrated the variation of the global properties of the system with the Lorentz transformations and have shown the discrepancies between the Newtonian approach and special relativity. However, less attention has been paid to the analysis of the changes on the global system characteristics derived from the escape basin topology. In the present work we have focused on describing the influence of the gravitational radius of the primaries on the metamorphosis of the exit basin topology and their consequences over the predictability of the asymptotic behavior of the system. We have demonstrated that the modification of the escape basin topology has a strong influence over relevant global properties of the system, such as the particle decay law, the uncertainty dimension, and the basin entropy. These properties are relevant since they give significant *a priori* information about the final fate of the system and its predictability.

The influence of the gravitational radius λ in the algebraic decay law of the particle has been highlighted, and a maximum at $\lambda \simeq 0.02$ related to the transformation of the escape basin topology with λ has been found. In the range $\lambda \in (0.02, 0.035]$ there is a rich variety of phenomena where we could find the creation and destruction of KAM islands.

Interestingly, the evolution of the uncertainty dimension, α, in a typical scattering function as the parameter λ is varied as been observed, and furthermore α decreases as λ increases. However, the results point out three different regions in the evolution of α with λ. First, there is a linear decay in the range $\lambda \in (0, 0.020)$. Then, at $\lambda \simeq 0.02$, there is an inflection point with a change in the slope of the decay. Later, there is an abrupt decay of the uncertainty dimension α, at $\lambda \simeq 0.0285$, that is, a crossover behavior. The evolution of the uncertainty dimension α varies with λ, and this has physical implications since that means that the asymptotic behavior of the system cannot be predicted in a direct and clear manner, but it varies in a nonlinear way, and we have provided a theoretical reasoning for it.

The use of the basin entropy S_b has helped us to quantify the evolution the complexity of the exit basins with the variations of the gravitational radius λ. All our results point out that the uncertainty in the prediction of the final fate of the system depends on the considered value of λ, and this relation is not monotonous. Curiously enough, S_b decreases linearly as λ grows in the range $\lambda \in (0, 0.02]$, while S_b evolves almost flat for $\lambda \in (0.02, 0.035]$.

According to the obtained results, when chaos is present, the escape basin topology may change with the addition of relativistic approximations, and this implies a higher difficulty to foresee the asymptotic behavior of the system. Therefore, we conclude that, in chaotic systems like this, one has to take into account the relativistic approach when we want to make accurate predictions about the final state, even when considering low velocities or weak gravitational fields.

There are some problems which may be approached using scenarios like the one described here. One could be interested in guessing the characteristics of a particle falling from the z axis towards a binary system, using post-Newtonian corrections as those presented here. If we write the gravitational radius in terms of the Schwarzschild radius R_s of one of the primaries, we have

$$\lambda = \frac{2km}{ac^2} = \frac{R_s}{a}. \tag{14}$$

Hence, if we model a particle of negligible mass approaching a binary system with $\lambda = 0.005$, the binary should have $a \sim 0.2 \times 10^3 R_s$. In physical units, when considering primaries

of $10M_\odot$, one should take $a \sim 10^{-3}R_\odot$, and we would be possibly facing a particle falling towards a stellar-mass black hole binary system once the inspiral phase has started towards the final coalescence. Another relevant result is that when λ is small, and the problem is close to the classical Newtonian limit, small changes in initial conditions still can lead to large changes in the global asymptotic behavior. Very small gravitational radii such as $\lambda = 5.0 \times 10^{-6}$ point to binaries that would have $a \sim 0.2 \times 10^6 R_s$. A primary with $m = 1.0M_\odot$ would make us consider $a \sim 10^{-1}R_\odot$. Here we may be modeling masses falling down towards a white dwarf binary.

Of course, the Sitnikov problem model is a very specific one, an overly clean case of the three-body problem. This is because it just aims to demonstrate how even the simplest case of the three-body problem can show a very complex behavior. However, the techniques presented here are of general interest and can be applied as a starting point for work on more complex and physical meaningful problems. These are quite interesting research topics to extend our current research.

ACKNOWLEDGMENTS

Fruitful discussions with Prof. Hans C. Ohanian are acknowledged. This work has been financially supported by the Spanish State Research Agency (AEI) and the European Regional Development Fund (ERDF, EU) under Projects No. FIS2016-76883-P and No. PID2019-105554GB-I00. L.H. has been supported by the NNSF of China under Grant No. 11775101.

[1] J. Barrow-Green, *The Princeton Companion to Mathematics* (Princeton University Press, Princeton, 2008).
[2] D. J. Griffiths, *Introduction to Quantum Mechanics* (Prentice Hall, Upper Saddle River, New Jersey, 2004).
[3] R. Crandall, R. Whitnell, and R. Bettenga, Am. J. Phys. **52**, 438 (1984).
[4] F. Calogero, J. Math. Phys. **10**, 2191 (1969).
[5] K. Sitnikov, Dokl. Akad. Nauk. USSR **133**, 303 (1960).
[6] R. Dvorak, F. Freistetter, and J. Kurths (eds), *Chaos and Stability in Planetary Systems* (Springer, New York, 2005).
[7] W. D. Heintz, *Double Stars* (Reidel, Dordrecht, 1978).
[8] Y. Guo and R. W. Farquhar, Acta Astronaut. **56**, 421 (2005).
[9] T. R. Lauer, S. Tremaine, E. A. Ajhar, R. Bender, A. Dressler, and S. M. Faber, Astrophys. J. **471**, L79 (1996).
[10] A. Celleti and V. Sidorenko, Celest. Mech. Dyn. Astron. **101**, 105C (2008).
[11] T. Kovács and B. Érdi, Celest. Mech. Dyn. Astron. **105**, 289 (2009).
[12] J. M. Seoane and M. A. F. Sanjuán, Rep. Prog. Phys. **76**, 016001 (2012).
[13] E. Ott and T. Tél, Chaos **3**, 417 (1993).
[14] C. Grebogi, E. Ott, and J. A. Yorke, Physica D **7**, 181 (1983).
[15] Y.-C. Lai and T. Tél, *Transient Chaos* (Springer, New York, 2011).
[16] C. Fidler, T. Tram, C. Rampf, R. Crittenden, K. Koyama, and D. Wands, J. Cosmol. Astropart. Phys. **12**, 022 (2017).
[17] S. Chandrasekhar, Astrophys. J. **142**, 1488 (1965).
[18] H. C. Ohanian, *Special Relativity: A Modern Introduction* (Physics Curriculum & Instruction, Lakeville, USA, 2001).
[19] M. Campanelli, C. O. Lousto, P. Marronetti, and Y. Zlochower, Phys. Rev. Lett. **96**, 111101 (2006).
[20] B. L. Lan, Chaos **16**, 033107 (2006).
[21] B. L. Lan, Chaos Solitons Fractals **42**, 534 (2009).
[22] B. L. Lan and F. Borondo, Phys. Rev. E **83**, 036201 (2011).
[23] S.-N. Liang and B. L. Lang, Results Phys. **4**, 187 (2014).
[24] J. D. Bernal, J. M. Seoane, and M. A. F. Sanjuán, Phys. Rev. E **95**, 032205 (2017).
[25] J. D. Bernal, J. M. Seoane, and M. A. F. Sanjuán, Phys. Rev. E **97**, 042214 (2018).
[26] T. Kovács, G. Bene, and T. Tél, Mon. Not. R. Astron. Soc. **414**, 2275 (2011).
[27] T. Damour and N. Deruelle, Ann. I.H.P.: Phys. Theor. **43**, 107 (1985).
[28] S. H. Bleher, C. Grebogi, E. Ott, and R. Brown, Phys. Rev. A **38**, 930 (1988).
[29] C. F. F. Karney, Physica D **8**, 360 (1983); B. V. Chirikov and D. L. Shepelyansky, **13**, 395 (1984); J. Meiss and E. Ott, *ibid.* **20**, 387 (1986); Y.-C. Lai, M. Ding, C. Grebogi, and R. Blümel, Phys. Rev. A **46**, 4661 (1992).
[30] C. Grebogi, S. W. McDonald, E. Ott, and J. A. Yorke, Phys. Lett. A **99**, 415 (1983).
[31] J. M. Seoane, M. A. F. Sanjuán, and Y.-C. Lai, Phys. Rev. E **76**, 016208 (2007).
[32] S. Bleher, E. Ott, and C. Grebogi, Phys. Rev. Lett. **63**, 919 (1989); S. Bleher, C. Grebogi, and E. Ott, Physica D **46**, 87 (1990).
[33] S. W. McDonald, C. Grebogi, E. Ott, and J. A. Yorke, Phys. Lett. D **17**, 125 (1985).
[34] C. Grebogi, H. E. Nusse, E. Ott, and J. A. Yorke, Lect. Notes Math. **1342**, 220 (1988); P. M. Battelino, C. Grebogi, E. Ott, and J. A. Yorke, Physica D **32**, 296 (1988).
[35] A. Daza, A. Wagemakers, B. Georgeot, D. Guéry-Odelin, and M. A. F. Sanjuán, Sci. Rep. **6**, 31416 (2016).
[36] A. R. Nieto, E. E. Zotos, J. M. Seoane, and M. A. F. Sanjuán, Nonlinear Dyn. **99**, 3029 (2020).